Title

Utility of quantitative measurement of T2 using restriction spectrum imaging for detection of clinically significant prostate cancer

Journal

Scientific Reports, 14(1)

ISSN

2045-2322

Authors

Rojo Domingo, Mariluz

Conlin, Christopher C

Karunamuni, Roshan

et al.

Publication Date

2024

DOI

10.1038/s41598-024-82742-8

Peer reviewed

scientific reports

Check for updates

OPEN

Utility of quantitative measurement of T_2 using restriction spectrum imaging for detection of clinically significant prostate cancer

Mariluz Rojo Domingo[1,2], Christopher C. Conlin[3], Roshan Karunamuni[2], Courtney Ollison[2], Madison T. Baxter[2], Karoline Kallis[2], Deondre D. Do[1,2], Yuze Song[2,4], Joshua Kuperman[3], Ahmed S. Shabaik[5], Michael E. Hahn[3], Paul M. Murphy[3], Rebecca Rakow-Penner[3], Anders M. Dale[3,6,7] & Tyler M. Seibert[1,2,3,8,9]✉

The Restriction Spectrum Imaging restriction score (RSIrs) has been shown to improve the accuracy for diagnosis of clinically significant prostate cancer (csPCa) compared to standard DWI. Both diffusion and T_2 properties of prostate tissue contribute to the signal measured in DWI, and studies have demonstrated that each may be valuable for distinguishing csPCa from benign tissue. The purpose of this retrospective study was to (1) determine whether prostate T_2 varies across RSI compartments and in the presence of csPCa, and (2) evaluate whether csPCa detection with RSIrs is improved by acquiring multiple scans at different TEs to measure compartmental T_2 (cT_2). Data includes two cohorts scanned for csPCa with 3T multi-*b*-value diffusion-weighted sequences acquired at multiple TEs. cT_2 values were computed from multi-TE RSI data and compared by compartment. CsPCa detection was compared between RSIrs and a logistic regression model (LRM) to predict the probability of csPCa using cT_2 in combination with RSI measurements. Two-sample t-tests ($\alpha = 0.05$) and the area under the receiver operating characteristic curve (AUC) were used for the statistical analyses. In both cohorts, T_2 was different ($p < 0.05$) across the four RSI compartments (*C1*, *C2*, *C3*, *C4*). Voxel-level, cohort 1: T_2 was different in csPCa for *C1*, *C2*, C_3 ($p < 0.001$). Patient-level, cohort 1: T_2 was different in csPCa patients in C_3 ($p = 0.02$); cohort 2: T_2 differed in csPCa patients in C_1 ($p = 0.01$), C_3 ($p = 0.01$) and *C4* ($p < 0.01$). Voxel-level csPCa detection: cT_2 did not improve discrimination over RSIrs alone ($p = 0.9$). Patient-level: RSIrs and the LRM performed better than diffusion alone ($p < 0.001$), but the difference in AUCs between RSIrs and the LRM was not significantly different ($p = 0.54$). In conclusion, significant differences in cT_2 were observed between normal and cancerous prostatic tissue. With our data, however, consideration of cT_2 in addition to diffusion did not significantly improve cancer detection performance.

Keywords Prostate, Cancer detection, T_2 mapping, Restriction spectrum imaging, Diffusion-weighted imaging

[1]Department of Bioengineering, University of California San Diego Jacobs School of Engineering, La Jolla, CA, USA. [2]Department of Radiation Medicine and Applied Sciences, University of California San Diego School of Medicine, La Jolla, CA, USA. [3]Department of Radiology, University of California San Diego School of Medicine, La Jolla, CA, USA. [4]Department of Electrical and Computer Engineering, University of California San Diego Jacobs School of Engineering, La Jolla, CA, USA. [5]Department of Pathology, University of California San Diego School of Medicine, La Jolla, CA, USA. [6]Department of Neurosciences, University of California San Diego School of Medicine, La Jolla, CA, USA. [7]Halıcıoğlu Data Science Institute, University of California San Diego, La Jolla, CA, USA. [8]Altman Clinical and Translational Research Institute, 9500 Gilman Drive, #0861, La Jolla, CA 92093, USA. [9]Department of Urology, University of California San Diego, La Jolla, CA, USA. ✉email: tseibert@health.ucsd.edu

Multiparametric magnetic resonance imaging (mpMRI) has become an important tool for the diagnosis of prostate cancer (PCa)[1]. MpMRI has proven to reduce unnecessary biopsies, mitigate overdiagnosis of clinically insignificant prostate cancer (indolent PCa), and enhance detection of clinically significant prostate cancer (csPCa, Grade Group ≥ 2)[2,3]. In standard reporting of prostate MRI (Prostate Imaging Reporting and Data System, PI-RADS v2.1[4]), diffusion-weighted imaging (DWI) and T_2 -weighted imaging are the principal modalities used to detect csPCa. DWI measures the random movement of water molecules within tissues, aiding in the visualization of areas of restricted diffusion associated with hypercellular csPCa[5]. Meanwhile, T_2 -weighted imaging provides detailed anatomical information and facilitates the visualization of abnormalities in prostate tissue. The combined analysis of these two sequences allows for a more in-depth evaluation of potential tumor lesions, thereby contributing to csPCa detection and characterization.

The challenge with the interpretation of conventional mpMRI lies in its inherent subjectivity and variability[6]. The interpretations of imaging data by different radiologists that rely on qualitative assessment alone leads to inconsistencies in the identification and characterization of csPCa lesions[7]. Interobserver variability significantly limits the accuracy and reliability of csPCa diagnosis[8]. To enhance diagnostic accuracy, there is a growing emphasis on the development and adoption of quantitative MRI approaches. Quantitative MRI aims to provide objective metrics of tissue properties associated with the probability of csPCa, offering the potential for more standardized and reproducible image assessment.

Restriction Spectrum Imaging (RSI) is a quantitative approach to DWI for csPCa detection and characterization. RSI scans are acquired at multiple *b*-values (diffusion weightings) to distinguish diffusion signal from tissue micro-compartments (intracellular water, extracellular hindered water, freely diffusing water, and flowing fluid)[9–12]. However, RSI models typically do not incorporate quantitative T_2 measurements. On the other hand, studies using luminal water imaging (LWI) and hybrid multidimensional MRI have shown that tissue T_2 can differ between prostate tissue compartments and provide diagnostic information that is complementary to diffusion[13,14].

In this study, we acquired prostate RSI data at multiple echo times (TEs) to measure compartmental T_2 in addition to diffusion. We aimed to determine whether compartmental T_2 (i.e., T_2 within each RSI micro-compartment) differs between cancerous and normal prostate tissue, and whether consideration of compartmental T_2 in RSI yields improved detection of csPCa.

Methods

Study population

This study was approved by the University of California San Diego (UCSD) institutional review board (IRB). All research was performed in accordance with relevant guidelines and regulations. An FDA-cleared, commercial version of RSI is used routinely in our center as part of clinical routine. The first cohort included 46 patients scanned for suspected or known PCa between August and December of 2016 with multiple TEs as part of a quality improvement project to determine the best TE. The second cohort included patients who were scanned for suspected or known PCa between March 2021 and January of 2023 with a multi-TE RSI protocol per clinical routine (the need to obtain informed consent was waived by the UCSD IRB for secondary use of routine clinical data) or after informed written consent as part of a clinical trial on treatment response assessment (clinicaltrials.gov NCT04349501). Patients were excluded if they had received any treatment for PCa prior to the MRI acquisition or if a lesion with PI-RADS score ≥ 3 was detected on MRI but no biopsy information was available.

Routine clinical evaluation

Patients in both cohorts underwent prostate MRI as part of routine clinical care for PCa, except for 38 patients in cohort 2 who were scanned as part of a prospective research study without clinical evaluation by a radiologist. MpMRI was performed according to PI-RADS guidelines, and interpretation was made per clinical routine using PI-RADS v2.1. Several patients, all from cohort 2, had PCa diagnosed on systematic biopsy without MRI, and then had an MRI with RSI before any treatment as part of a prospective study; PI-RADS scores are not available for these subjects. PI-RADS interpretation was done as part of clinical practice, but the original lesion segmentations were not available for the present study. Those segmentations are made in routine clinical practice using a proprietary software for biopsy that does not permit exporting the lesions. The radiologists in the present study segmented all biopsy-confirmed lesions, relying on the images themselves and the written description of those biopsy targets provided in the routine clinical PI-RADS reports. The presence of clinically significant prostate cancer (csPCa, grade group ≥ 2) was determined from biopsy results, typically systematic 12-core biopsy with additional targeted cores for suspicious lesions on MRI. Patients with PI-RADS lesions of 1 or 2 with no biopsy were considered negative for csPCa, in accordance with European Association of Urology (EAU) guidelines[15–17].

RSI data acquisition and processing

All patients were scanned with an expanded MRI protocol that included two multi-*b*-value RSI acquisitions performed with different TEs. MRI acquisition details are summarized in Table 1. All MR imaging was performed on a 3T clinical scanner (Discovery MR750; GE Healthcare, Waukesha, WI, USA), using a 32-channel phased-array coil over the pelvis. For each patient, two axial, multi-*b*-value DWI volumes were separately acquired using two different TEs: 80 ms and 100 ms for cohort 1, and 76 ms and 90 ms for cohort 2. All other parameters were the same between scans. In addition to the DWI volumes, a single T_2-weighted volume was acquired for anatomical reference using the same scan coverage as the DWI volumes. MRI post-processing was performed using programs implemented in MATLAB R2022a (MathWorks, Natick, MA, USA[18]). DWI volumes were corrected to account for B_0-inhomogeneities, gradient nonlinearities, eddy currents[19], and image noise[10].

Cohort 1	DWI 1	DWI 2	T_2-weighted
Pulse sequence	EPI*	EPI*	FSE†
TR (ms)	5000	5000	6225
TE (ms)	80	100	100
FOV (mm)	220 × 220	220 × 220	220 × 220
Matrix [resampled dimensions]	96 × 96 [128 × 128]	96 × 96 [128 × 128]	320 × 320 [512 × 512]
Slices	34	34	34
Slice Thickness (mm)	3	3	3
b-values (s/mm^2) [number of samples]	0[7‡], 200 [6], 1000 [6], 2000 [6], 3000 [6]	0[7‡], 200 [6], 1000 [6], 2000 [6], 3000 [6]	N/A
Cohort 2	**DWI 1**	**DWI 2**	**T_2-weighted**
Pulse sequence	EPI*	EPI*	FSE†
TR (ms)	4500	4500	6230
TE (ms)	76	90	98
FOV (mm)	20 × 100	200 × 100	200 × 200
Matrix [resampled dimensions]	80 × 48 [128 × 128]	80 × 48 [128 × 128]	320 × 320 [512 × 512]
Slices	32	32	32
Slice Thickness (mm)	3	3	3
b-values (s/mm^2) [number of samples]	0 [2‡], 50[6], 800[6], 1500[12], 3000 [18]	0 [2‡], 50[6], 800[6], 1500[12], 3000 [18]	N/A

Table 1. Acquisition details for DWI and T_2-weighted image volumes. All MR imaging was performed on a 3T clinical scanner (Discovery MR750; GE Healthcare), using a 32-channel phased-array coil over the pelvis. The two DWI volumes for both cohorts were acquired using different TEs to allow for examination of T_2 relaxation in prostatic tissue compartments. The single T_2-weighted volume was acquired for anatomical reference. *Diffusion-weighted echo-planar imaging. †Fast spin echo. ‡An extra $b = 0\ \mathrm{s/mm^2}$ volume was acquired with reverse phase encoding to enable correction of B_0-inhomogeneity distortions.

Samples at each b-value were averaged together. Image registration[20] was applied to correct for patient motion between acquisitions.

For patients in cohort 1, regions of interest (ROIs) were manually defined on T_2-weighted images over the whole prostate, peripheral zone, and transition zone (the central zone was included with the transition zone). The contouring of the prostate zones and tumor lesions was performed using MIM software (MIM software version 7.2.6, Inc; Cleveland, OH, USA[21]), by a radiation oncologist with 3 years of experience and two board-certified sub-specialist radiologists with 4 and 6 years of experience, using all available clinical imaging and pathologic information[11]. Radiologist-certified contours of the prostate zones and lesions were not obtainable for cohort 2. Instead, automated prostate contours, which are generally highly accurate[22], were obtained using an FDA-cleared commercial product (OnQ Prostate version 1.4, CorTechs.ai, San Diego, CA, USA[23]).

RSI modeling

Prior studies established and validated a four-compartment RSI model of the diffusion signal[10,11,24]:

$$S(b) = \sum_{i=1}^{4} C_i e^{-bD_i}$$

$S(b)$ denotes the measured DWI signal intensity at a particular b-value, which is modeled as a linear combination of exponential decays representing four diffusion compartments. C_i describes the compartmental signal contributions to be determined via model-fitting. The diffusion coefficients, D_i, are fixed for each of the four tissue compartments to empirically determined values[10] that broadly represent restricted diffusion, hindered diffusion, free diffusion, and vascular flow: 1.1e−4, 1.8e−3, 3.6e−3, and 0.1220 mm^2/s, respectively. Signal-contribution (C_i) maps were computed for both DWI volumes per patient by fitting this model to the signal-vs.-b-value curve from each voxel. A previously validated biomarker for PCa called the RSI restriction score (RSIrs) was computed by dividing the signal intensity of the restricted diffusion compartment, C_1, at each voxel by the median signal intensity within the whole prostate on the $b = 0$ mm^2/s DWI images (an index of apparent T_2-weighting in the prostate)[11,24–27].

Compartmental T_2 mapping and analysis by csPCa status

T_2 maps were computed for each compartment of the RSI model by fitting the monoexponential T_2 decay formula to the signal values from the two C_i maps with different TEs. The median T_2 within the whole prostate was then computed. Two-sample t-tests ($\alpha = 0.05$) were used to determine whether there were significant differences in median T_2 between compartments.

For cohort 1, two-sample t-tests ($\alpha = 0.05$) were used to compare median compartmental T_2 values between benign or clinically insignificant PCa tissue and csPCa lesions. For both cohorts, we used two-sample t-tests ($\alpha = 0.05$) to compare each patient's median T_2 by compartment in the whole prostate, and whether

compartmental T_2 was significantly different between patients with and without csPCa. Any compartments with a significant difference in T_2 between normal and cancerous tissue were noted for inclusion in subsequent multivariable modeling.

Logistic regression model fitting and evaluation of cancer-detection performance

A logistic regression model (LRM) was developed to estimate the probability that a given voxel of tissue contains csPCa given measurements of diffusion and compartmental T_2. RSIrs[11] was included as the diffusion parameter of the model. Compartmental T_2 was included in the LRM for each compartment that showed a significant difference in T_2 between normal and cancerous tissue. Cohort 1 had radiologist-certified lesion contours available and was therefore used to train the LRM. In patients with csPCa, voxels inside the lesion contours were labeled as csPCa-positive, while prostate voxels outside the lesion contours were labeled as csPCa-negative. In these patients, voxels labeled as csPCa-positive were included to train the LRM and all non-csPCa voxels were excluded. In patients without csPCa, diffusion and compartmental T_2 measurements from all voxels within the entire prostate were used to train the LRM and labeled as csPCa-negative.

Ten-fold cross-validation was performed to evaluate voxel-level csPCa-detection performance of the model within cohort 1. We assessed csPCa-detection performance using the area under the receiver operating characteristic curve (AUC) and calculated 95% confidence intervals (CI) from 10,000 bootstrap samples.

Both cohorts were used to test the patient-level csPCa-detection performance of the model. For patient-level analysis of the LRM, the highest probability value observed within the whole prostate was used as the predictor variable. Similarly, the maximum RSIrs value within the whole prostate was used as the patient-level predictor for RSIrs. We also computed maximum C_1 to obtain the patient-level performance of diffusion only, as RSIrs incorporates global prostate T_2 signal in addition to diffusion signal. AUC values were computed for maximum C_1, maximum RSIrs, and the LRM, and compared using two-sample t-tests ($\alpha = 0.05$). The 95% confidence intervals were estimated through random sampling with replacement from 10,000 bootstrap patient samples.

Results

Study population

Cohort 1 comprised 46 patients (age: 70 ± 10 years; PSA: 10.6 ± 16.9 ng/mL). Cohort 2 comprised 195 patients (age: 69 ± 8 years; PSA: 8.2 ± 8.5 ng/mL). In cohort 1, 22 of 46 patients (47.8%) had csPCa, while the remaining 24 had either low-grade (grade group 1) disease or no cancer. In cohort 2, 96 of 195 (49.2%) patients had csPCa. 38 participants from cohort 2 had no PI-RADS scores available because csPCa was diagnosed on systematic biopsy without MRI and then had an MRI with RSI acquisition as part of a separate, prospective study. Table 2 summarizes the patient characteristics of both cohorts.

Compartmental T_2 mapping

Figure 1 shows compartmental T_2 maps for two patients with csPCa, one from each cohort.

Figure 2 shows violin plots of median T_2 within the whole prostate for each RSI model compartment. In both cohorts, the highest median T_2 values were observed in C_3, followed by C_2, C_4, and finally C_1. Compartmental T_2 was significantly different between any two compartments ($p < 0.05$).

Voxel-level analysis of compartmental T_2 values by csPCa status

For each compartment of the RSI model, the comparison of T_2 values between csPCa and prostate tissue outside of csPCa lesions is illustrated in Fig. 3. This figure corresponds to cohort 1, which has radiologist-certified csPCa lesion contours. csPCa lesions showed significantly higher compartmental T_2 values in compartment 1 ($p << 0.001$) and compartment 2 ($p << 0.001$) than normal tissue. In addition, the compartmental T_2 values of compartment C_3 were significantly lower in csPCa lesions ($p << 0.001$). The compartmental T_2 values for compartment C_4 were not significantly different between csPCa and normal tissues ($p = 0.17$).

Patient-level analysis of compartmental T_2 values by csPCa status

The comparison of compartmental T_2 values between patients with and without csPCa is shown in Fig. 4. In both cohorts, patients with csPCa had higher compartmental T_2 values in compartment C_1 than patients with no csPCa. In cohort 2, median C_1 compartmental T_2 was significantly higher ($p = 0.07$ for cohort 1; $p = 0.01$ for cohort 2). Median C_3 compartmental T_2 was significantly different between csPCa and patients without csPCa in both cohorts ($p = 0.02$ for cohort 1; $p = 0.01$ for cohort 2). Median C_4 compartmental T_2 was also significantly different in cohort 2 ($p << 0.01$). Compartmental T_2 values for the other compartments were not significantly different between patients with and without csPCa.

Logistic regression model fitting and evaluation of csPCa-detection performance

T_2 measurements from RSI compartments 1, 2, and 3 (C_1, C_2, C_3) were included as the T_2 parameters of the LRM. These three compartments showed significantly different median T_2 signal between csPCa lesions vs csPCa-negative voxels. The LRM predictors were RSIrs, C_1-T_2, C_2-T_2, and C_3-T_2. The model coefficients with 95% confidence interval for the y-intercept and RSIrs were 6.367 (6.323, 6.416) and -51.621 (-52.354, -50.888), respectively. The weights for C_1-T_2, C_2-T_2, and C_3 T_2 were < 0.005. Example probability maps computed from the model are shown in Fig. 5 for two patients with csPCa, alongside maps of RSIrs.

Voxel-level cancer detection

For voxel-level cancer detection, the tenfold cross-validation mean AUC of the LRM was 0.98 [95% CI: 0.957–0.985], versus 0.98 [95% CI: 0.958–0.986] for maximum RSIrs, indicating that incorporating compartmental T_2 did not improve discrimination over RSIrs alone ($p = 0.9$).

Cohort 1 (n = 46)		
Available pathology	Systematic biopsy only	6
	Targeted Biopsy Only	0
	Systematic and targeted biopsy	20
	Prostatectomy	15
	No biopsy or prostatectomy*	5
PI-RADS	1	9
	2	2
	3	10
	4	10
	5	15
	Not available	0
Gleason grade group	Benign	17
	1	2
	2	9
	3	8
	4	1
	5	4
Cohort 2 (n = 195)		
Available pathology	Systematic biopsy only	44
	Targeted Biopsy Only	5
	Systematic and targeted biopsy	60
	Prostatectomy	28
	No biopsy or prostatectomy**	31
PI-RADS	1	66
	2	10
	3	18
	4	36
	5	27
	Not available†	38
Gleason grade group	Benign	38
	1	30
	2	40
	3	32
	4	7
	5	17

Table 2. Summary of radiologic and pathologic characteristics of the two cohorts of patients included in this study. *4 patients had PI-RADS 1 scores, and 1 patient had PI-RADS 2 scores. **27 patients had PI-RADS 1 scores, and 4 patients had PI-RADS 2 scores. †Part of a prospective research study without clinical evaluation by a radiologist.

Patient-level cancer detection

For cohort 1, the AUC of the LRM was 0.804 [0.648–0.930], versus 0.805 [0.648–0.931] for RSIrs. The mean AUC for maximum C_1 was 0.695 [0.530–0.851]. The difference in AUCs between RSIrs and the multivariable model was not significantly different ($p = 0.26$). Both RSIrs and the LRM performed significantly better than diffusion (maximum C_1) alone (both $p << 0.001$).

For cohort 2, the mean LRM AUC for 10,000 bootstrapped samples was 0.724 [0.650–0.793]. The mean AUC of RSIrs for 10,000 bootstrapped samples was 0.725 [0.652–0.794]. For maximum C_1 the mean AUC was 0.654 [0.573, 0.730]. The difference in AUCs between RSIrs and the multivariable model was not significantly different ($p = 0.54$). Both RSIrs and the LRM performed significantly better than diffusion (maximum C_1) alone (both $p << 0.001$). ROC curves for both cohorts are shown in Fig. 6.

Discussion

We found that compartmental T_2 values were significantly different across RSI diffusion compartments. Moreover, compartmental T_2 values differed between csPCa lesions and benign tissue or low-grade PCa in RSI compartments C_1, C_2, and C_3. At the patient level, there were also differences in whole-prostate T_2 between patients with no csPCa and those with biopsy-proven csPCa. Quantitative differences in compartmental T_2 may provide insight into the microstructural changes associated with PCa. For example, extracellular matrix remodeling may contribute to the increased compartmental T_2 observed in C_2[12]. Lower compartmental T_2

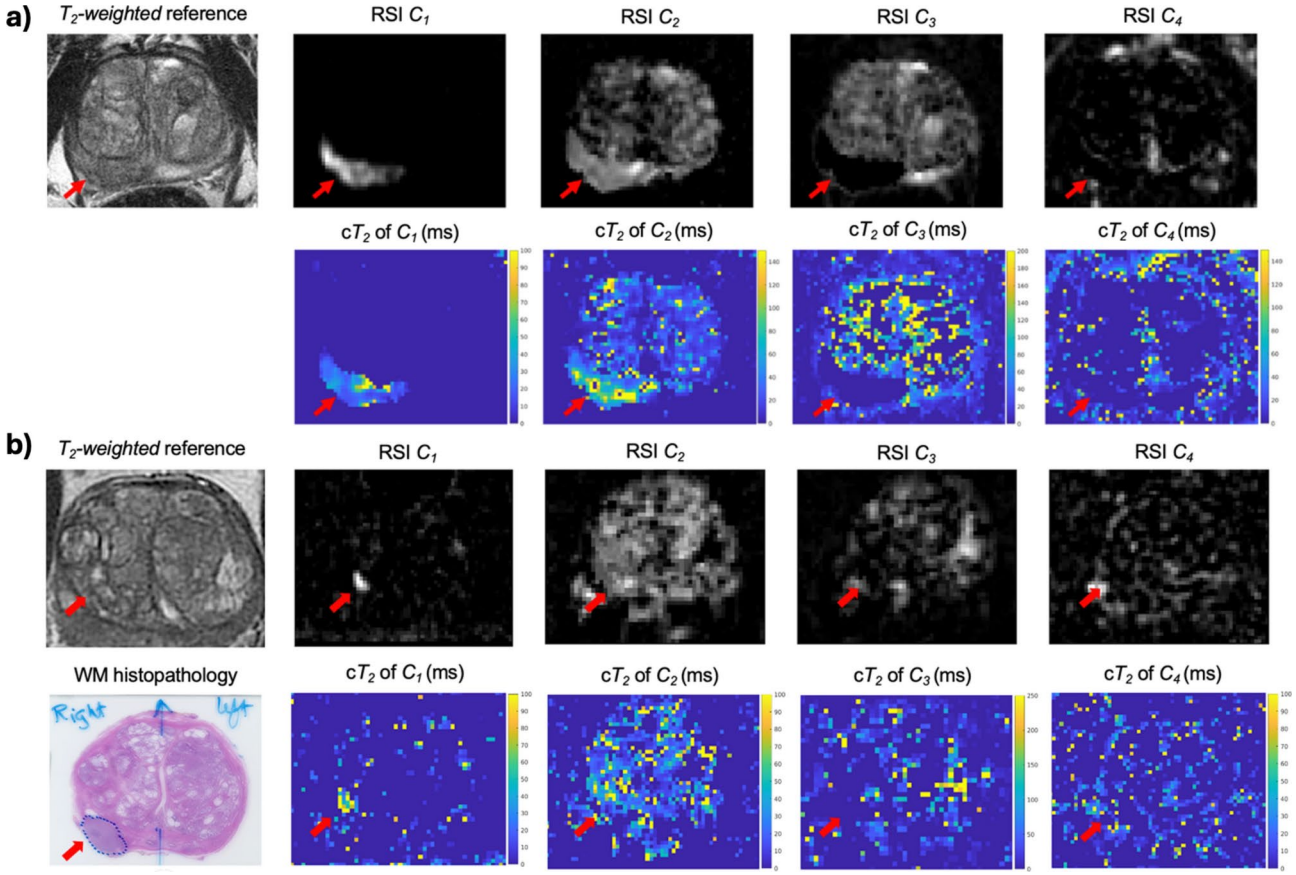

Fig. 1. RSI signal contribution (C_i) and compartmental T_2 (cT_2) maps for two patients with csPCa. (**A**) Patient from cohort 1. (**B**) Patient from cohort 2. Compartmental T_2 maps were computed for each RSI model compartment by measuring the T_2 -weighted signal decay of the signal-contribution map for different TEs. The signal-contribution maps shown here were computed from the DWI acquisition with shorter TE. Whole-mount (WM) histopathology results were available for the patient from cohort 2 and illustrate the lesion contour in the prostate. For cohort 1, the contouring of the prostate zones and tumor lesions was performed using MIM software (MIM software version 7.2.6, Inc; Cleveland, OH, USA[21]). For cohort 2, automated prostate contours were obtained using an FDA-cleared commercial product (OnQ Prostate version 1.4, CorTechs.ai, San Diego, CA, USA[23]).

values in C_3 may reflect hyperplasia-induced reductions in luminal space[13]. While the elevated compartmental T_2 observed in C_1 of csPCa patients may seem opposed to the known overall hypointense appearance of csPCa on T_2-weighted MRI, it is consistent with an increase in nuclear volume fraction that is typical of cancer cells[28].

We have previously shown that RSIrs is a useful quantitative DWI biomarker for csPCa at the voxel- and patient-level[11,24,26]. Here, we evaluated whether incorporating compartmental T_2 values would improve csPCa discrimination over RSIrs alone. We demonstrated that T_2 effects have csPCa discriminatory value, as they showed higher AUC values compared to diffusion alone in both cohorts. However, consideration of compartmental T_2 did not significantly improve csPCa-detection performance over maximum RSIrs at the voxel- or patient-level. This finding may suggest an overlap of microstructural information that is captured by diffusion and T_2-weighted imaging. A number of studies have demonstrated an interdependence between apparent diffusion coefficient (ADC) measurements and T_2 values[29,30]. Diffusion measurements from RSI and T_2 measurements from techniques like Luminal Water Imaging (LWI) are both also strongly correlated with microstructural tissue features, including cellularity and luminal water space, that are indicative of cancer[31]. It may be that the RSI and T_2 measurements in this study both reflect similar aspects of tissue microstructure, and their combination therefore does not yield a substantial increase of diagnostically useful information[32].

As with any conventional DWI acquisition, signal from the individual RSI compartments is also partially T_2-weighted. RSIrs further incorporates a measure of global T_2-weighted signal in the prostate, namely the median signal within the prostate on the $b=0$ s/mm^2 volume. These T_2-weighting factors intrinsic to RSIrs are correlated with the values obtained from quantitative T_2-mapping, so the addition of T_2-mapping may not have provided sufficiently complementary information to improve csPCa discrimination performance.

Other advanced imaging techniques have also been used to measure T_2 in the prostate. LWI utilizes the unique T_2 relaxation rates associated with various components of prostate tissue to quantify the fractional volume of glandular lumen, denoted as luminal water fraction (LWF)[33]. This method takes advantage of the

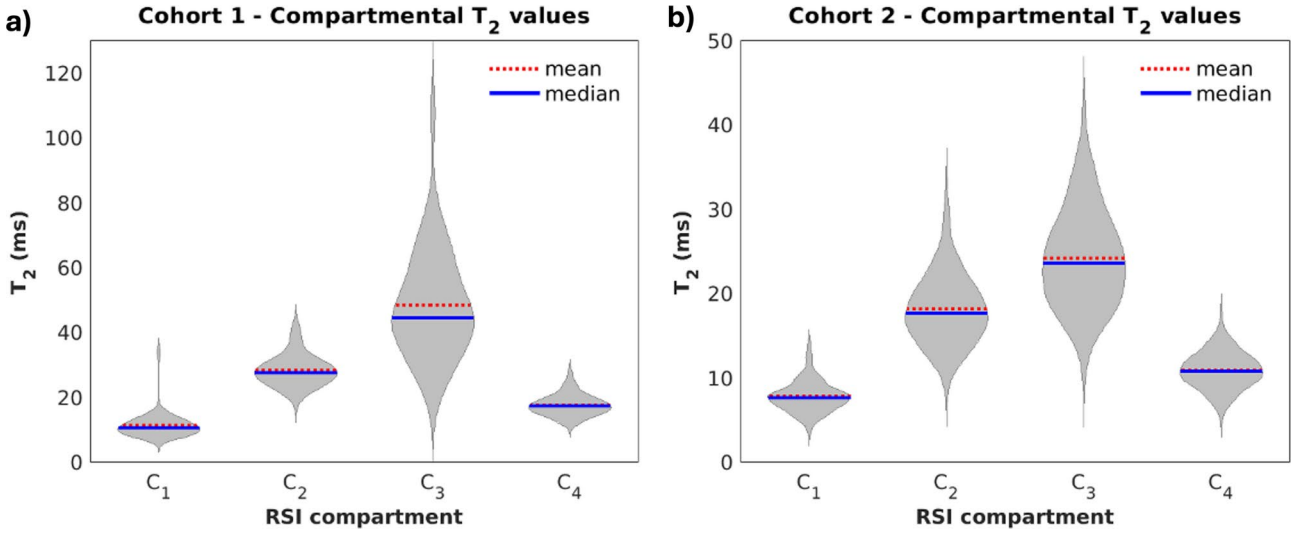

Fig. 2. Violin plots showing the distribution of median T_2 values in the whole prostate for each of the four RSI model compartments. Within each cohort, compartmental T_2 was significantly different between any two compartments ($p < 0.05$). (**A**) cohort 1 (n = 46). (**B**) cohort 2 (n = 195). Plots were created using MATLAB R2022a (MathWorks, Natick, MA, USA[18]). For cohort 1, the contouring of the prostate zones and tumor lesions was performed using MIM software (MIM software version 7.2.6, Inc; Cleveland, OH, USA[21]). For cohort 2, automated prostate contours were obtained using an FDA-cleared commercial product (OnQ Prostate version 1.4, CorTechs.ai, San Diego, CA, USA[23]).

observed alterations in the composition of prostatic tissue in the presence of cancer and the Gleason grade of the cancer for PCa diagnosis[31]. Hybrid multidimensional MRI (HM-MRI) exploits the interdependence of T_2 and ADC values to measure prostate volume fractions of the lumen, epithelium, and stroma[34]. Studies using LWI and HM-MRI demonstrate lower T_2 values in cancer lesions compared to normal prostate tissue with increasing Gleason Grade. The decrease in T_2 results from a decrease in luminal volume due to cellular hyperplasia[31,35]. This trend agrees with the decrease observed in this study of T_2 in compartment C_3 of patients with csPCa. This RSI compartment reflects signal from freely diffusing water in the prostate, which we expect to find predominantly in luminal tissue and to be impacted by a reduction in luminal space. Prior work with HM-MRI showed that the decrease in luminal space is largely the result of epithelial tissue proliferation, indicated by an increase in the measured epithelial volume fraction[34]. Since RSI does not explicitly assign signal contributions to a particular tissue type, this aspect of HM-MRI is harder to align with the present study. However, we can be sure that the changes observed in the T_2 of compartment C_1 reflect, at least in part, an increase in the overall tissue cellularity[36]. Signal contributions in this compartment are also dependent upon the nuclear volume fraction of cells in the tissue[28], and the increase in the T_2 observed in C_1 of csPCa patients suggests an increase in nuclear volume fraction.

While quantitative T_2 did not yield improved patient-level csPCa discrimination compared to RSI alone, the ROI-based analysis of this study suggests that it may be helpful for lesion-level detection and characterization of tumors at a microscopic level. Whole-mount histopathology (WMHP) data are currently being collected as part of an ongoing study to map changes in compartmental RSI signal to the histological restructuring of prostate tissue due to csPCa. This mapping aims to correlate RSI and T_2 signal with specific microscopic alterations observed in tumors. This approach could also aid in identifying variations in T_2 across different tumor grades, providing a non-invasive means to predict grade group and assess the aggressiveness of cancer[13], a crucial prognostic indicator. Another ongoing, prospective trial (ART-Pro; NCT06579417) is evaluating the impact of RSIrs and compartmental T_2 on csPCa diagnosis in a heterogeneous multi-center and multi-reader dataset[37].

Future work that pairs RSI with a more advanced, multicompartmental approach to T_2 measurement, such as LWI, would allow for deeper insight into the relationship between compartmental diffusion and T_2 than was achievable here. Our acquisition protocol involved only a sparse sampling of two TEs compared to 5 b-values, while LWI would provide many more TE measurements to enable a more granular assessment of the T_2 microenvironment. This would help determine whether diffusion and T_2 measurements truly provide complementary information about the prostate and serve to enhance csPCa detection accuracy when used together.

Limitations

The use of separate acquisitions and only two TEs per patient may have limited the accuracy of voxel-wise compartmental T_2 measurements. However, the inclusion of additional TEs was restricted to avoid excessive protocol length on active clinical scanners.

While other quantitative MRI approaches use lower TEs (< 30 ms) for T_2 mapping[14,31], the high b-values required by RSI to optimally estimate C_1 are generally incompatible with very low TEs on clinical scanners.

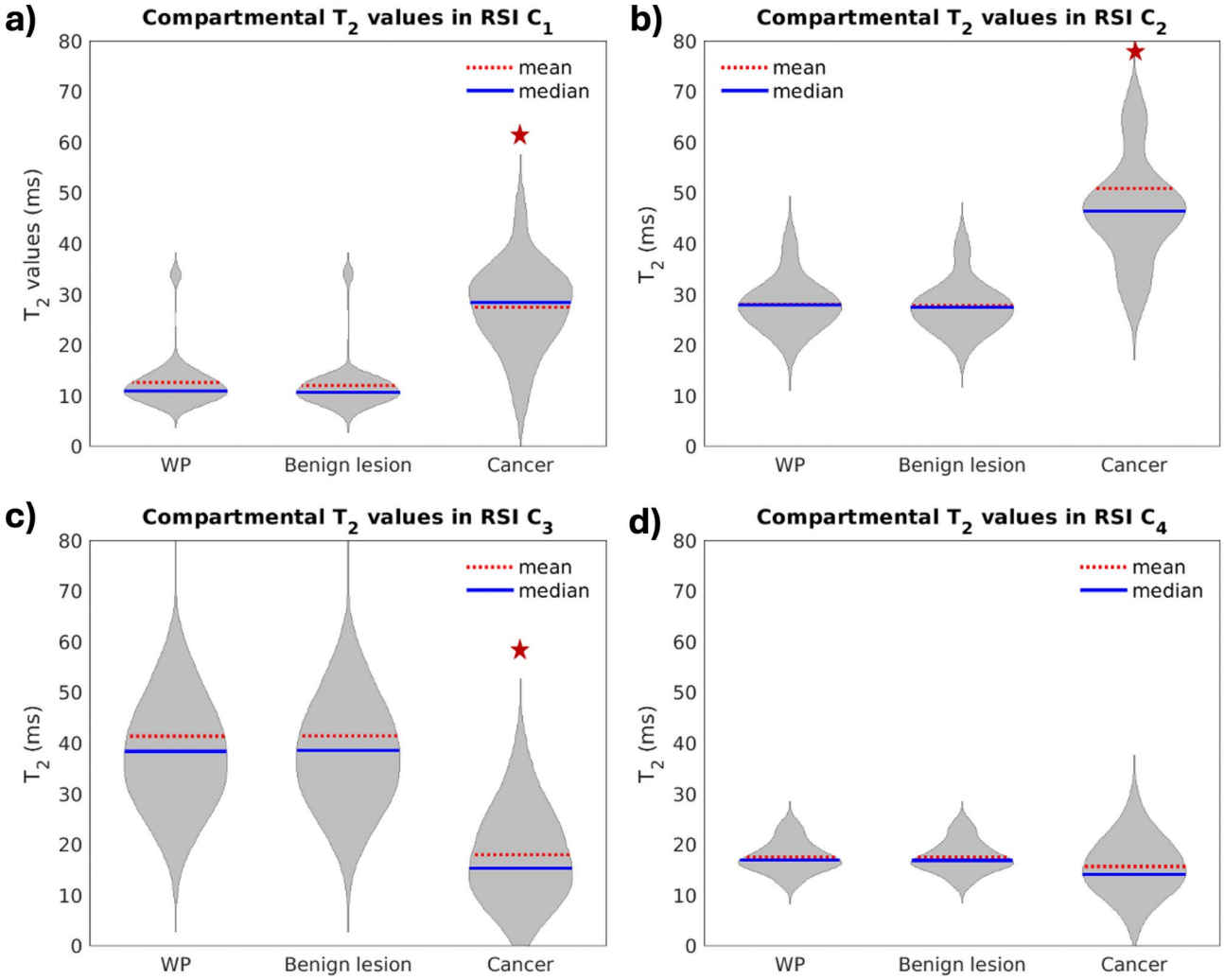

Fig. 3. Violin plots showing the distribution of median compartmental T_2 values from cohort 1 in both csPCa lesions and the surrounding prostate tissue. Each panel corresponds to one of the RSI diffusion compartments. csPCa lesions showed significantly higher compartmental T2 values in C_1 (p-value $<<0.001$) and C_2 (p-value $<<0.001$) than tissues outside of csPCa lesions. Compartmental T_2 values of C_3 were also significantly lower in csPCa lesions than outside csPCa lesions (p-value $<<0.001$). A red star indicates a significant difference (p-value <0.05) in compartmental T_2 between csPCa lesions and the prostate tissue outside the lesions. WP: whole prostate. Plots were created using MATLAB R2022a (MathWorks, Natick, MA, USA[18]). For cohort 1, the contouring of the prostate zones and tumor lesions was performed using MIM software (MIM software version 7.2.6, Inc; Cleveland, OH, USA[21]).

Separate acquisitions would therefore be required to evaluate the combination of optimal RSIrs and T_2 estimated with very low TE. Another limitation of this study is that our voxel-level data included only high-confidence csPCa and control categories, leaving little room for improvement over RSIrs for the voxel-level analysis[11].

Conclusion

T_2 mapping affords insights into characteristics of benign and cancerous prostate tissue, but we did not find compelling evidence that acquisitions with multiple TE is necessary for patient-level csPCa detection with RSI.

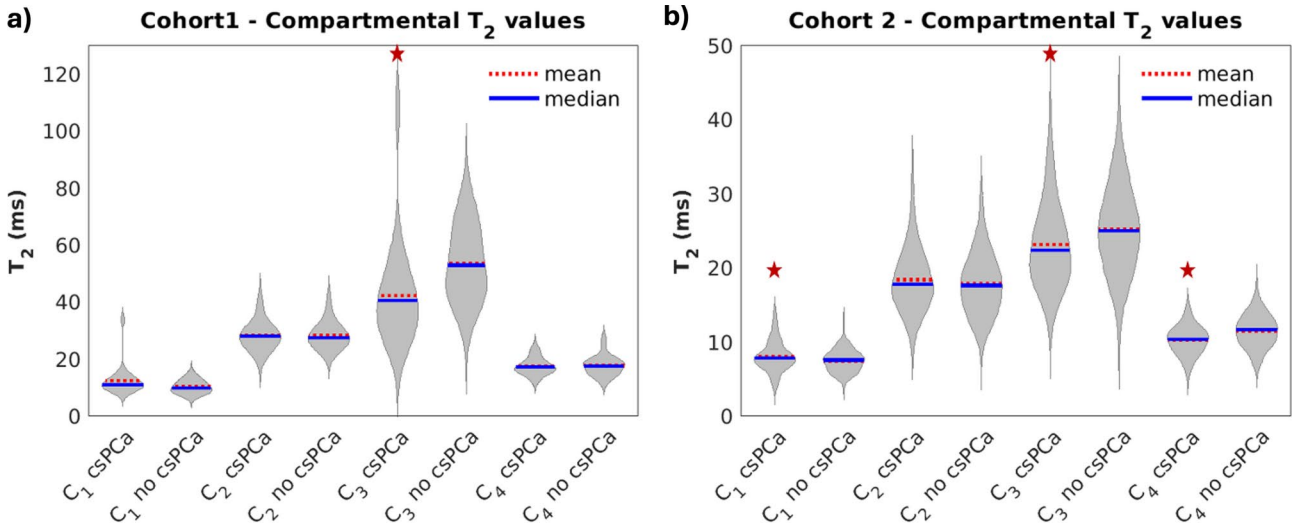

Fig. 4. Violin plots comparing compartmental T_2 within the whole prostate between patients with csPCa and those without. A red star indicates a significant difference (p-value < 0.05) in whole-prostate compartmental T_2 between csPCa and non-csPCa patients. (**A**) cohort 1 (n = 46). (**B**) cohort 2 (n = 195). Plots were created using MATLAB R2022a (MathWorks, Natick, MA, USA[18]). For cohort 1, the contouring of the prostate zones and tumor lesions was performed using MIM software (MIM software version 7.2.6, Inc; Cleveland, OH, USA[21]). For cohort 2, automated prostate contours were obtained using an FDA-cleared commercial product (OnQ Prostate version 1.4, CorTechs.ai, San Diego, CA, USA[23]).

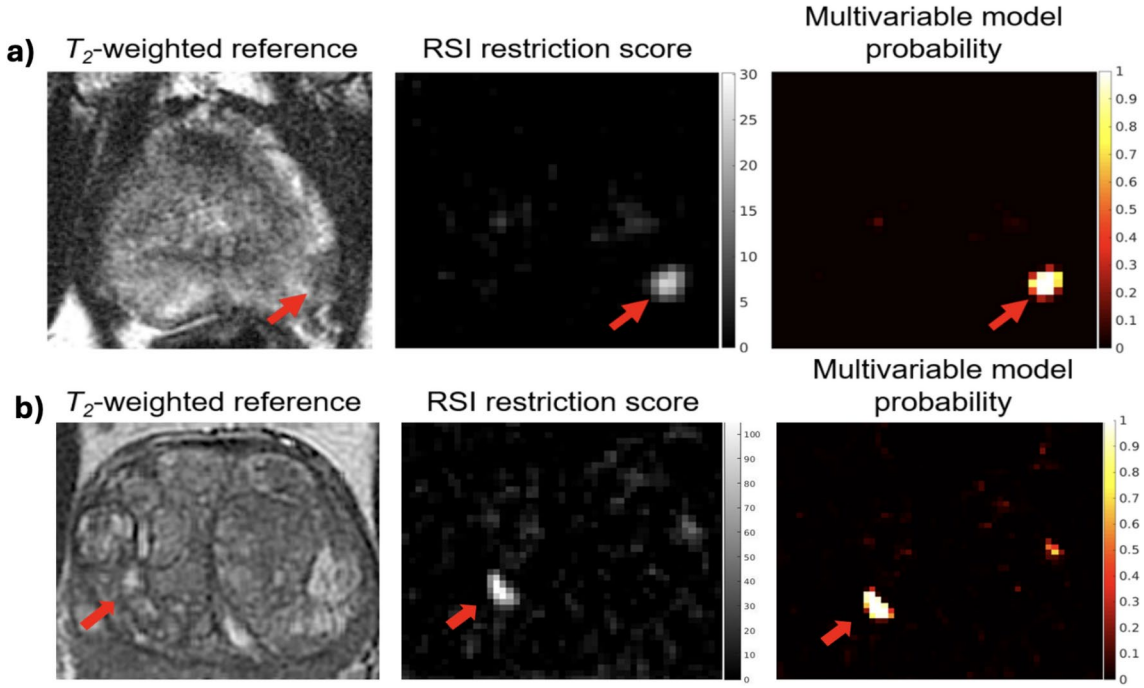

Fig. 5. RSI restriction score and multivariable model probability maps of the prostate for patients with csPCa. Top panel: Patient from cohort 1 with a lesion in the left peripheral zone. Bottom panel: Patient from cohort 2 with a lesion in the transition zone. The multivariable model uses compartmental T_2 measurements from each voxel in addition to the RSI restriction score to determine the probability that it contains csPCa. For the patient from cohort 1, the contouring of the prostate zones and tumor lesions was performed using MIM software (MIM software version 7.2.6, Inc; Cleveland, OH, USA[21]). For patient from cohort 2, automated prostate contours were obtained using an FDA-cleared commercial product (OnQ Prostate version 1.4, CorTechs.ai, San Diego, CA, USA[23]).

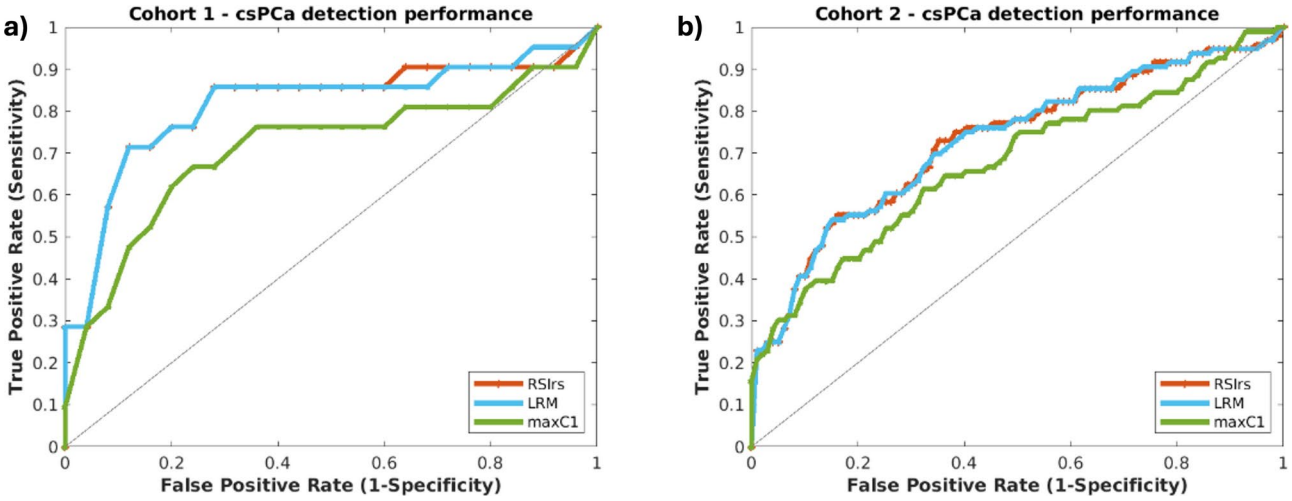

Fig. 6. Patient-level diagnostic performance of maximum RSIrs, the LRM and maximum C_1 (max C_1) for cohorts 1 and 2. (**A**) For cohort 1, mean AUC values were 0.695 for maximum C_1, 0.805 for RSIrs and 0.804 for the multivariable model. (**B**) For cohort 2, mean AUC values were 0.654 for maximum C_1, 0.725 for RSIrs and 0.724 for the multivariable model. Plots were created using MATLAB R2022a (MathWorks, Natick, MA, USA[18]). For cohort 1, the contouring of the prostate zones and tumor lesions was performed using MIM software (MIM software version 7.2.6, Inc; Cleveland, OH, USA[21]). For cohort 2, automated prostate contours were obtained using an FDA-cleared commercial product (OnQ Prostate version 1.4, CorTechs.ai, San Diego, CA, USA[23]).

Data availability

Data are available for bona fide researchers who request it from the authors. Please contact Dr. Tyler Seibert (tseibert@health.ucsd.edu) if you would like to request the data from this study.

Received: 5 June 2024; Accepted: 9 December 2024
Published online: 28 December 2024

References

1. Leung, D.K.-W., Chiu, P.K.-F., Ng, C.-F. & Teoh, J.Y.-C. Role of pre-biopsy multiparametric MRI in prostate cancer diagnosis: Evidence from the literature. *Turk. J. Urol.* **47**(Suppl 1), S65–S70. https://doi.org/10.5152/tud.2020.20360 (2021).
2. de Rooij, M., Hamoen, E. H. J., Fütterer, J. J., Barentsz, J. O. & Rovers, M. M. Accuracy of multiparametric MRI for prostate cancer detection: A meta-analysis. *AJR Am. J. Roentgenol.* **202**(2), 343–351. https://doi.org/10.2214/AJR.13.11046 (2014).
3. Schoots, I. G. et al. Magnetic resonance imaging-targeted biopsy may enhance the diagnostic accuracy of significant prostate cancer detection compared to standard transrectal ultrasound-guided biopsy: A systematic review and meta-analysis. *Eur. Urol.* **68**(3), 438–450. https://doi.org/10.1016/j.eururo.2014.11.037 (2015).
4. Scott, R., Misser, S. K., Cioni, D. & Neri, E. PI-RADS v2.1: What has changed and how to report. *SA J. Radiol.* **25**(1), 2062. https://doi.org/10.4102/sajr.v25i1.2062 (2021).
5. Demirel, H. C. & Davis, J. W. Multiparametric magnetic resonance imaging: Overview of the technique, clinical applications in prostate biopsy and future directions. *Turk. J. Urol.* **44**(2), 93–102. https://doi.org/10.5152/tud.2018.56056 (2018).
6. Pickersgill, N. A. et al. Accuracy and variability of prostate multiparametric magnetic resonance imaging interpretation using the prostate imaging reporting and data system: A blinded comparison of radiologists. *Eur. Urol. Focus* **6**(2), 267–272. https://doi.org/10.1016/j.euf.2018.10.008 (2020).
7. Midiri, F., Vernuccio, F., Purpura, P., Alongi, P. & Bartolotta, T. V. Multiparametric MRI and radiomics in prostate cancer: A review of the current literature. *Diagn. Basel Switz.* **11**(10), 1829. https://doi.org/10.3390/diagnostics11101829 (2021).
8. Stabile, A. et al. Factors influencing variability in the performance of multiparametric magnetic resonance imaging in detecting clinically significant prostate cancer: A systematic literature review. *Eur. Urol. Oncol.* **3**(2), 145. https://doi.org/10.1016/j.euo.2020.02.005 (2020).
9. Brunsing, R. L. et al. Restriction spectrum imaging: An evolving imaging biomarker in prostate MRI: Prostate MRI with restriction spectrum imaging: A review. *J. Magn. Reson. Imaging* **45**(2), 323–336. https://doi.org/10.1002/jmri.25419 (2017).
10. Conlin, C. C. et al. Improved characterization of diffusion in normal and cancerous prostate tissue through optimization of the restriction spectrum imaging signal model. *Radiol. Imaging* https://doi.org/10.1101/2020.03.27.20042069 (2020).
11. Feng, C. H. et al. Voxel-level classification of prostate cancer on magnetic resonance imaging: Improving accuracy using FOUR-compartment restriction spectrum imaging. *J. Magn. Reson. Imaging* **54**(3), 975–984. https://doi.org/10.1002/jmri.27623 (2021).
12. White, N. S. et al. Diffusion-weighted imaging in cancer: Physical foundations and applications of restriction spectrum imaging. *Cancer Res.* **74**(17), 4638–4652. https://doi.org/10.1158/0008-5472.CAN-13-3534 (2014).
13. Hectors, S. J., Said, D., Gnerre, J., Tewari, A. & Taouli, B. Luminal water imaging: Comparison With diffusion-weighted imaging (DWI) and PI-RADS for characterization of prostate cancer aggressiveness. *J. Magn. Reson. Imaging* **52**(1), 271–279. https://doi.org/10.1002/jmri.27050 (2020).
14. Chatterjee, A. et al. Diagnosis of prostate cancer with noninvasive estimation of prostate tissue composition by using hybrid multidimensional MR imaging: A feasibility study. *Radiology* **287**(3), 864–873. https://doi.org/10.1148/radiol.2018171130 (2018).

15. EAU Guidelines on Prostate Cancer—Uroweb. Uroweb - European Association of Urology. Accessed: Oct. 16, 2023. [Online]. https://uroweb.org/guidelines/prostate-cancer
16. Abdul Raheem, R. et al. Can a prostate biopsy be safely deferred on PI-RADS 1,2 or 3 lesions seen on pre-biopsy mp-MRI?. *Arab. J. Urol.* **21**(1), 10–17. https://doi.org/10.1080/2090598X.2022.2119711 (2023).
17. Reijnen, J. S. et al. Results from a PI-RADS-based MRI-directed diagnostic pathway for biopsy-naive patients in a non-university hospital. *Abdom. Radiol. N. Y.* **46**(12), 5639–5646. https://doi.org/10.1007/s00261-021-03249-8 (2021).
18. "MATLAB." Accessed: Nov. 19, 2024. [Online]. https://www.mathworks.com/products/matlab.html
19. Holland, D., Kuperman, J. M. & Dale, A. M. Efficient correction of inhomogeneous static magnetic field-induced distortion in Echo Planar Imaging. *NeuroImage* **50**(1), 175–183. https://doi.org/10.1016/j.neuroimage.2009.11.044 (2010).
20. Paquin, D., Levy, D., Schreibmann, E. & Xing, L. Multiscale image registration. *Math. Biosci. Eng.* **3**(2), 389–418 (2006).
21. MIM Software Inc. | Precision Care Simplified. Accessed: Nov. 17, 2024. [Online]. http://mimsoftware-5300642.hs-sites.com
22. Y. Song *et al.* Precise prostate contours: Setting the bar and meticulously evaluating AI performance. https://doi.org/10.1101/2024.10.21.24315771 (2024).
23. "OnQ^{TM} Prostate - Cortechs.ai." Accessed: Nov. 14, 2024. [Online]. https://www.cortechs.ai/solution/onq-prostate/
24. Zhong, A. Y. et al. Automated patient-level prostate cancer detection with quantitative diffusion magnetic resonance imaging. *Eur. Urol. Open Sci.* **47**, 20–28. https://doi.org/10.1016/j.euros.2022.11.009 (2023).
25. Conlin, C. C. et al. Background prostate tissue is quantitatively abnormal on MRI in patients with clinically significant prostate cancer. *Radiol. Imaging* https://doi.org/10.1101/2022.10.12.22280855 (2022).
26. Lui, A. J. et al. ReIGNITE RT boost: An international study testing the accuracy and feasibility of using restriction spectrum imaging (RSI) MRI to guide intraprostatic tumor target volume for radiotherapy boost. *Oncology* https://doi.org/10.1101/2022.12.13.22283420 (2022).
27. Kallis, K. et al. Comparison of synthesized and acquired high b-value diffusion-weighted MRI for detection of prostate cancer. *Radiol. Imaging* https://doi.org/10.1101/2023.02.17.23286100 (2023).
28. White, N. S. & Dale, A. M. Distinct effects of nuclear volume fraction and cell diameter on high b-value diffusion MRI contrast in tumors: Diffusion in Tumor Cells. *Magn. Reson. Med.* **72**(5), 1435–1443. https://doi.org/10.1002/mrm.25039 (2014).
29. Sadinski, M. et al. Pilot study of the use of hybrid multidimensional T2-weighted imaging–DWI for the diagnosis of prostate cancer and evaluation of Gleason score. *Am. J. Roentgenol.* **207**(3), 592–598. https://doi.org/10.2214/AJR.15.15626 (2016).
30. Wang, S. et al. Hybrid multidimensional T2 and diffusion-weighted MRI for prostate cancer detection. *J. Magn. Reson. Imaging JMRI* **39**(4), 781. https://doi.org/10.1002/jmri.24212 (2013).
31. Sabouri, S. et al. Luminal water imaging: A new MR imaging T2 mapping technique for prostate cancer diagnosis. *Radiology* **284**(2), 451–459. https://doi.org/10.1148/radiol.2017161687 (2017).
32. Hepp, T. et al. T2 mapping for the characterization of prostate lesions. *World J. Urol.* **40**(6), 1455. https://doi.org/10.1007/s00345-022-03991-8 (2022).
33. Chatterjee, A., Harmath, C. & Oto, A. New prostate MRI techniques and sequences. *Abdom. Radiol.* **45**(12), 4052–4062. https://doi.org/10.1007/s00261-020-02504-8 (2020).
34. Lee, G. H. et al. Comparing radiologist performance in diagnosing clinically significant prostate cancer with multiparametric versus hybrid multidimensional MRI. *Radiology* **305**(2), 399–407. https://doi.org/10.1148/radiol.211895 (2022).
35. Chatterjee, A. et al. Changes in epithelium, stroma, and lumen space correlate more strongly with Gleason pattern and are stronger predictors of prostate ADC changes than cellularity metrics. *Radiology* **277**(3), 751–762. https://doi.org/10.1148/radiol.2015142414 (2015).
36. Liss, M. A. et al. MRI-derived restriction spectrum imaging cellularity index is associated with high grade prostate cancer on radical prostatectomy specimens. *Front. Oncol.* https://doi.org/10.3389/fonc.2015.00030 (2015).
37. M. T. Baxter *et al.* 2024 Advanced Restriction imaging and reconstruction Technology for Prostate MRI (ART-Pro): Study protocol for a multicenter, multinational trial evaluating biparametric MRI and advanced, quantitative diffusion MRI for detection of prostate cancer. *medRxiv* https://doi.org/10.1101/2024.08.29.24311575 (2024).

Acknowledgements

This work was supported, in part, by the National Institutes of Health (NIH/NIBIB K08EB026503, NIH UL-1TR000100), the American Society for Radiation Oncology, the Prostate Cancer Foundation (PCF20YOUN01), and the U.S. Department of Defense (DOD/CDMRP PC220278).

Author contributions

M.R.D. and C.C.C. contributed equally to the work. Drafting of the manuscript: M.R.D., C.C.C., T.M.S. Statistical Analyses, Conception and Design: M.R.D., C.C.C., R.K., T.M.S. Data acquisition: C.O., M.T.B., D.D.D., M.R.D., C.C.C., T.M.S. Manuscript revision: all authors. Corresponding Author: T.M.S.

Declarations

Competing interests

M.E.H. reports honoraria from Multimodal Imaging Services Corporation and research funding from GE Healthcare. R.R.P. has an equity interest in CorTechs Labs and Curemetrix, serves on the scientific advisory board of Imagine Scientific, and has received consulting fees from Bayer and research funding from GE Healthcare. A.M.D. is a founder of and holds equity in CorTechs Labs, Inc, and serves on its scientific advisory board; he also is a member of the scientific advisory board of Human Longevity, Inc, and receives funding through research agreements with GE Healthcare. T.M.S. reports honoraria from CorTechs Labs, Varian Medical Systems, WebMD, GE Healthcare, and Janssen; has an equity interest in CorTechs Labs, Inc, and serves on its scientific advisory board; and has received in-kind research support from GE Healthcare via a research agreement with the University of California, San Diego. These companies might potentially benefit from the research results. The terms of these arrangements have been reviewed and approved by the University of California, San Diego in accordance with its conflict-of-interest policies. All the remaining authors declare no conflict of interest.

Additional information

Correspondence and requests for materials should be addressed to T.M.S.